Received: 22 August 2022 | Revised: 18 November 2022 | Accepted: 8 December 2022

DOI: 10.1002/mawe.202200184

ARTICLE

WILEY VCH

On ascertaining hardness-microstructure relationship in annealed steel for varying carbon content

Ermittlung der Härte-Gefüge-Beziehung in geglühtem Stahl bei unterschiedlichem Kohlenstoffgehalt

J. Maity | **S. A. Rahman** | **S. Alam** | **K. K. Singh** | **P. Kumar** | **S. Hembram**

Department of Metallurgical and Materials Engineering, National Institute of Technology Durgapur, Durgapur, West Bengal, India

Correspondence
J. Maity, Department of Metallurgical and Materials Engineering, National Institute of Technology Durgapur, Durgapur 713209, West Bengal, India.
Email: joydeep.maity@mme.nitdgp.ac.in and joydeep_maity@yahoo.co.in

Abstract

Plain carbon steels of five different carbon contents up to eutectoid composition have been provided with the conventional full annealing treatment. Qualitative and quantitative studies of the microstructure are carried out using optical microscopy and field emission scanning electron microscopy techniques. Even under similar cooling rate pertaining to the full annealing treatment (furnace cooling); microstructural modifications of individual microconstituents are feasible with varying chemistry (carbon content) of plain carbon steel. The refinement of microstructure for both proeutectoid α-ferrite and pearlite is found to be accentuated with increasing carbon content of annealed steels till eutectoid composition. Hall-Petch type relationship explains adequately the relationship between hardness and the size of the microconstituent both in terms of the grain size of proeutectoid α-ferrite and the interlamellar spacing of pearlite. Henceforth an empirical relationship is developed for the first time taking into account the rule of mixture to correlate overall hardness, carbon content, grain size of proeutectoid α-ferrite and interlamellar spacing of pearlite. The empirical relationship originated thereby is found to closely match the experimental results.

KEYWORDS
annealing treatment, chemistry-structure-property correlation, empirical relationship, plain carbon steel, varying carbon content

SCHLÜSSELWÖRTER
Chemie-Gefüge-Eigenschafts-Korrelation, empirische Beziehung, Glühbehandlung, unlegierter Kohlenstoffstahl, unterschiedlicher Kohlenstoffgehalt

1 | INTRODUCTION

The iron-carbon system appears to be one of the most intriguing systems in nature that not only accommodates three invariant reactions, but also sustains a variety of solid state phase transformations to nurture the most popular engineering material called 'steel'. Amidst significant development and dramatic turnaround being experienced over more than ten decades, evolved microconstituents as a consequence of phase transformations

https://doi.org/10.1002/mawe.202200184

of wide diversity in steel seem to be never-ending; starting from δ-ferrite, austenite, α-ferrite, bainite, martensite, lamellar pearlite, non-lamellar/degenerated pearlite and so on. The diverse gamut of microstructure originated thereby manifests to provide properties in a wide range essentially compatible to the necessary application for mankind. The inherent science pertinent to steel technology broadly classifies solid state phase transformation in steel into two categories; namely, reconstructive transformation and displacive transformation [1, 2]. As a part of prime technological process, when steel is austenitized first (thereby evolving single phase polycrystalline austenite phase) to provide further treatment in the form of cooling at various rates, various possibilities of phase transformation at solid state gain certainty depending on the subsequent cooling schedule adopted. Accordingly, austenite may transform to pearlite as a consequence of reconstructive transformation involving diffusion as well as interfacial reaction [3, 4]. In contrast, Widmanstätten ferrite evolves from austenite by virtue of diffusion-assisted displacive transformation [5]. Moreover, martensite is a diffusionless displacive transformation product; while bainitic transformation being also displacive, involves diffusion during paraequilibrium nucleation and remains diffusionless during growth [6, 7]. As a part of technological advancement, instead of initial complete austenitization, an incomplete austenitization to stabilize fragmented cementite particles in a matrix of austenite followed by cooling at various rates for a single or multiple cycles has been initiated in last decade [8–12]. This encounters various forms of divorced eutectoid structure, often altogether termed as the 'degenerated pearlite' [13–16]. Apart from thermal treatment, the feasibility of various solid state phase transformations (including evolution of martensite) in steel has been verified recently with high-voltage low-current electric energy input [17–19].

Therefore, the vast diversity in various microstructural features as a consequence of solid state phase transformations in steel extends a feasibility of contemplation in a wide domain of knowledge-bases even at its very basic level not dealt with so far. In this regard, in case of most common complete austenitization based heat treatment, the morphology of two prime microconstituents (namely, proeutectoid α-ferrite and pearlite) originated from the parent austenite phase in hypoeutectoid steel is believed to be only dependent on cooling rate. In other words, irrespective of chemistry, 'fine' or 'coarse' morphological existence of microconstituents is only correlated to the rate of cooling executed [20, 21]. The manifestation of such structural modification in terms of impact on mechanical property is usually ascertained by Hall-Petch type equation [22–24]. When present corresponding author contemplated upon this aspect fundamentally, the effect of varying chemistry in view of changing carbon content in various hypoeutectoid steels would appear to have an effect on the structural refinement of proeutectoid α-ferrite and pearlite, since the 'transformation temperature' vis-à-vis the 'degree of undercooling' is likely to be affected by the shift of time-temperature-transformation diagram. Incidentally, this aspect has not been studied till date. Conceiving this unresolved techno-scientific issue, the present research work is formulated in studying the structural modifications in plain carbon steel for varying carbon content under a particular cooling rate (pertaining to annealing) in view of chemistry-structure-property correlation phenomenology. Accordingly, in this research work plain carbon steel of five different carbon contents up to eutectoid composition are subjected to conventional full annealing treatment. Qualitative and quantitative studies of the microstructures are carried out using optical microscopy and field emission scanning electron microscopy techniques. Overall hardness and hardness values of individual microconstituents are measured. Finally, an empirical relationship is developed to correlate overall hardness, carbon content, grain size of proeutectoid α-ferrite and interlamellar spacing of pearlite. The novelty of this research work stems from conceiving the microstructural variation in steel even for similar cooling rate with varying carbon content and the ultimate development of a unique empirical relationship for chemistry-structure-property correlation.

2 | EXPERIMENTAL PROCEDURE

2.1 | Material

The materials selected for the present investigation were plain carbon steels of varying carbon content; namely, 0.05 weight% carbon, 0.192 weight% carbon, 0.35 weight% carbon, 0.48 weight% carbon and 0.79 weight% carbon. The chemical composition of these steels was analysed by an optical emission spectrometer (Q4 Tasman, Bruker Elemental GmbH, Germany), Table 1.

2.2 | Heat treatment

Small pieces of chosen steels of dimension: 12 mm × 12 mm × 12 mm were subjected to conventional full annealing treatment in an electric resistance furnace of ±2 °C temperature accuracy. This full annealing

TABLE 1 Chemical composition of different steels.

Steel designation	Chemical composition (weight %)										
	C	Mn	Si	Ni	Cr	Mo	P	S	V	W	Fe
AISI 1005	0.05	0.292	0.024	0.014	nil	0.0019	0.02	0.018	0.00085	0.049	balance
AISI 1020	0.192	0.74	0.062	0.0081	0.0072	0.0085	0.018	0.027	0.0015	0.017	balance
AISI 1035	0.35	0.779	0.246	0.165	0.093	0.031	0.017	0.023	0.0021	nil	balance
AISI 1050	0.48	0.77	0.20	nil	0.04	nil	0.02	0.01	nil	nil	balance
AISI 1080	0.79	0.73	0.33	0.07	0.10	0.03	0.023	0.005	nil	nil	balance

TABLE 2 Austenitizing temperature of different steels.

Steel designation	A_3 (°C)	A_1 (°C)	T_A (°C)
AISI 1005	867	Not required	917
AISI 1020	824	Not required	874
AISI 1035	800	Not required	850
AISI 1050	778	Not required	828
AISI 1080	Not required	719	769

treatment involved heating to a desired temperature (T_A) pertaining to fully austenitic region, holding at this temperature isothermally for 1 hour and subsequent furnace cooling to the room temperature. The desired austenitizing temperature (T_A) is considered as ($A_3 + 50$)°C for hypoeutectoid steels (0.05 weight% carbon, 0.192 weight% carbon, 0.35 weight% carbon and 0.48 weight% carbon steels) and as ($A_1 + 50$) °C for eutectoid steel (0.79 weight% carbon steel). The upper critical temperature (A_3) and the lower critical temperature (A_1) are calculated using the standard formula mentioned in literature [25]. These are narrated below.

A_1 (in °C) = 723 − 20.7 × (weight % manganese) − 6.9 × (weight % nickel) + 29.1 × (weight % silicon) + 16.9 × (weight % chromium) + 290 × (weight % arsenic) + 6.38 × (weight % tungsten).

A_3 (in °C) = 910 − 203 × (weight % carbon)$^{1/2}$ − 15.2 × (weight % nickel) + 44.7 × (weight % silicon) + 104 × (weight % vanadium) + 31.5 × (weight % molybdenum) + 13.1 × (weight % tungsten).

The detailed calculation of austenitizing temperature (T_A) is accordingly summarized, Table 2. Furthermore, the cooling curves (temperature-time history) pertaining to furnace cooling for different steels have been recorded, Figure 1.

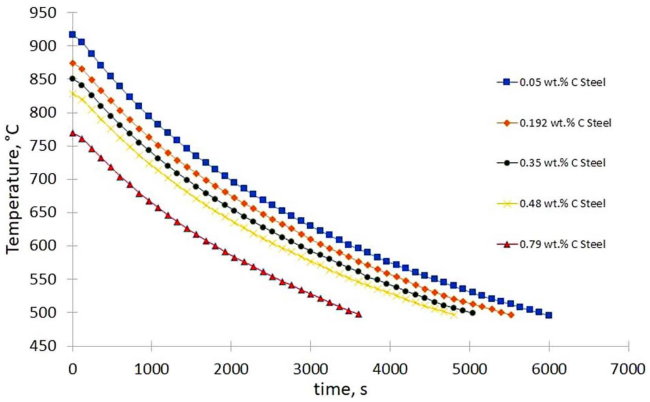

FIGURE 1 Furnace cooling curves for different steels.

2.3 | Optical metallography

The annealed specimens were at first subjected to rough grinding operation (up to a depth of 2 mm) to remove surface oxide and decarburized layer and thereafter subjected to standard metallographic specimen preparation steps. These steps involved fine grinding in emery paper up to 1000 grit size, cloth polishing with fine alumina abrasive followed by etching with 2% nital. These metallographic specimens were studied in a metallurgical optical microscope (Leica, DM 2700 M) equipped with quantitative image analysis software (LAS V4.8) for qualitative as well as quantitative interpretation. Quantitative

analysis of photomicrographs involved determination of the volume fraction of different microconstituents (proeutectoid α-ferrite and pearlite) and determination of grain size of the proeutectoid α-ferrite phase. The grain size of the proeutectoid α-ferrite phase is determined following the ASTM E 112 standard in terms of average grain diameter (D) [26].

2.4 | Field emission scanning electron microscopy

The metallographic specimens were further studied in a field emission scanning electron microscope (Model: SIGMA, Zeiss, Germany). In particular the interlamellar spacing of the pearlite is adequately revealed and measured accordingly from field emission scanning electron micrographs.

2.5 | Microhardness test

The Vickers hardness values of individual microconstituents (proeutectoid α-ferrite and pearlite) in different specimens were measured using a microhardness testing machine (MMT-X7B, Hibiki Co. Japan) at 25 gf load (HV 0.025). Besides, overall Vickers hardness values of all the specimens were measured using the same machine at 2 kgf load (HV 2).

3 | RESULTS AND DISCUSSION

3.1 | Evolution of microstructure

The optical micrographs of the annealed steel specimens of varying carbon content are interpreted, Figure 2a–e. With regard to existing conceptualization, hypoeutectoid steels primarily contain proeutectoid α-ferrite and pearlite as the two prime microconstituents, Figure 2a–d. On the other hand, the eutectoid steel contains primarily pearlite where proeutectoid α-ferrite phase is negligible, Figure 2e.

Furthermore, the quantitative analysis taken up onto these optical micrographs delineates the volume fraction of two prime microconstituents (proeutectoid α-ferrite and pearlite) and grain size of proeutectoid α-ferrite, respectively, Tables 3, 4. Corresponding graphical representation of the volume fraction of two microconstituents and the grain size of proeutectoid α-ferrite are also inspected, Figures 3, 4. It is interesting to note that the relative proportion of proeutectoid α-ferrite decreases and the proportion of pearlite increases with increase in carbon content of hypoeutectoid steels. The prevailing situation in the present case of furnace

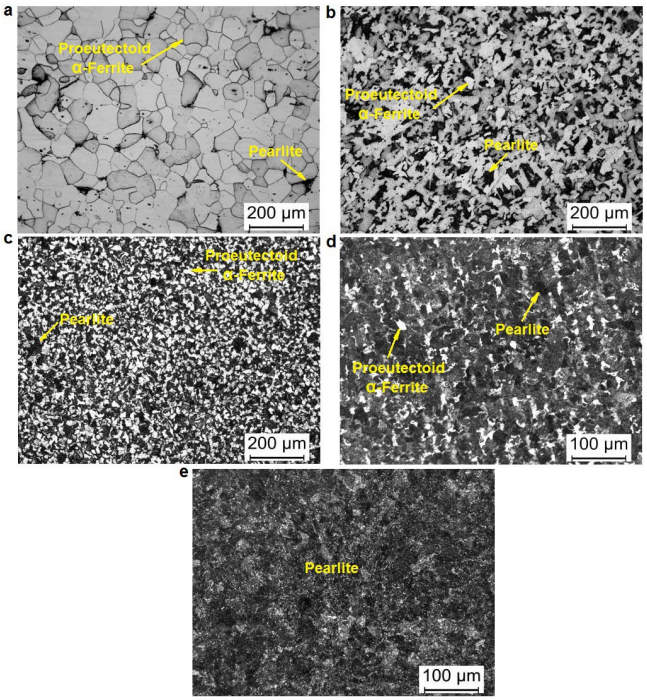

FIGURE 2 Optical micrographs of annealed steels containing (a) 0.05 wt.% C, (b) 0.192 wt.% C, (c) 0.35 wt.% C, (d) 0.48 wt.% C, and (e) 0.79 wt.% C.

TABLE 3 Volume fraction of prime microconstituents in different annealed steels.

Steel designation	Carbon content, (weight %)	Measured volume fraction of proeutectoid α-ferrite	Measured volume fraction of pearlite	Volume fraction of proeutectoid α-ferrite as per Lever rule	% deviation of the volume fraction of proeutectoid α-ferrite with respect to Lever rule
AISI 1005	0.05	0.967	0.033	0.968	0.1
AISI 1020	0.192	0.773	0.227	0.785	1.5
AISI 1035	0.35	0.567	0.433	0.581	2.4
AISI 1050	0.48	0.449	0.551	0.413	8.7
AISI 1080	0.79	Negligible	1	Negligible	Negligible

TABLE 4 Grain size of proeutectoid α-ferrite in different annealed steels.

Steel designation	Carbon content, (weight %)	Average grain diameter (D), (μm)
AISI 1005	0.05	60.3
AISI 1020	0.192	50.7
AISI 1035	0.35	28.2
AISI 1050	0.48	21.9
AISI 1080	0.79	Not applicable

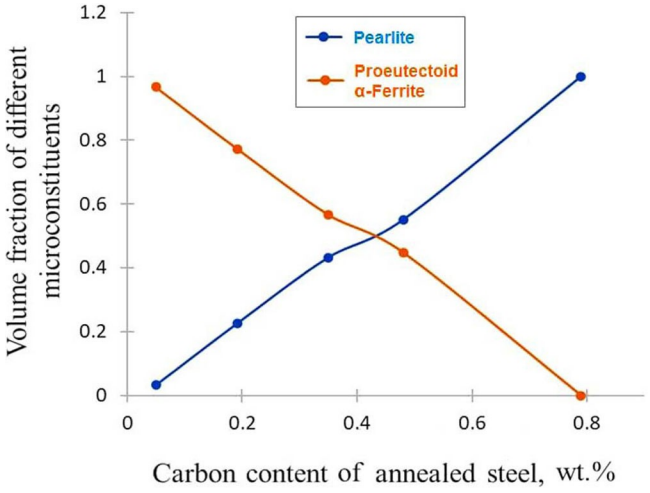

FIGURE 3 Variation of the measured volume fraction of different microconstituents with carbon content of annealed steels.

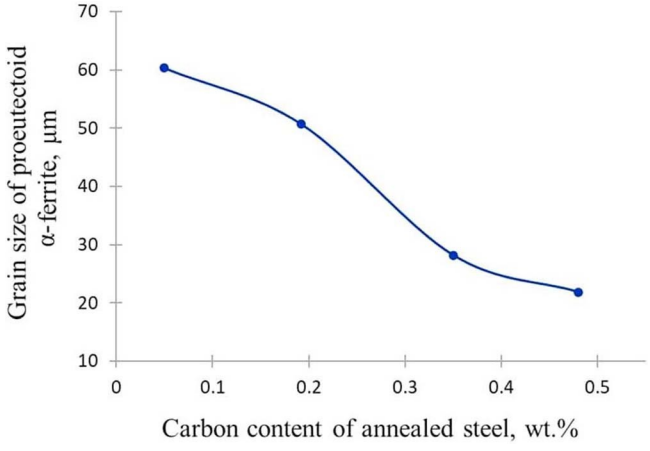

FIGURE 4 Variation of the measured grain size of proeutectoid α-ferrite with carbon content of annealed steels.

cooling rate being closer to equilibrium cooling (extremely slow cooling), this effect is easily realized in terms of application of so-called Lever rule. In this regard, following well known relationships may be considered as per Lever rule.

The fraction of proeutectoid α-ferrite,

$$f_{PF} = \left(\frac{0.8 - X}{0.8 - 0.025}\right) \quad (1)$$

$$\text{The fraction of pearlite, } f_p = \left(\frac{X - 0.025}{0.8 - 0.025}\right) \quad (2)$$

Where X is the weight% carbon present in steel. Accordingly, a decline in the fraction of proeutectoid α-ferrite and an increase in the fraction of pearlite are observed with increasing carbon content. The volume fraction of proeutectoid α-ferrite, as measured from optical photomicrographs through quantitative metallography technique, does not deviate much (% deviation <10) from that calculated using lever rule, Equation 1, Table 3. Relatively more deviation (though less than 10%) towards higher carbon content is plausibly accounted for the presence of other alloying elements, manganese in particular. The application of Lever rule, with a primary origin from mass balance, should be treated as an analytical approach. Therefore, less than 10% deviation is quite reasonable considering the presence of other alloying elements within the domain of plain carbon steel. Furthermore, grain size of the proeutectoid α-ferrite decreases with increase in carbon content of hypoeutectoid steel, thereby indicating structural refinement, Table 4. Further exemplification of structural refinement is envisaged on introspection of high resolution field emission scanning electron micrographs in terms of the reduction in the interlamellar spacing (λ) of the pearlite with an increase in carbon content, Table 5, Figures 5, 6, 7. Moreover, in view of an adequate agreement between microstructural observation and graphical representation, it appears that the more pronounced decline of interlamellar spacing (at nano-scale) with increasing carbon content is observed for lower carbon content than that for higher carbon content, Figures 6, 7.

The overall structural refinement in terms of grain size reduction in the proeutectoid α-ferrite region as well as reduction in the interlamellar spacing of the pearlite region even for similar slow rate of cooling (furnace cooling) has not been reported so far in existing literature. Almost in all literature available hitherto, the effect of faster cooling rate (say in case of normalizing as compared to annealing) on structural refinement of steel has been reported [20, 21, 27, 28]. However, in the present research work the structural refinement effect under similar rate of slow furnace cooling (slope of cooling curves being almost same) may be explained on introspection of time-temperature-transformation diagram with respect to carbon content of steel up to eutectoid composition, Figure 8. It is fundamentally known that

TABLE 5 Interlamellar spacing of pearlite in different annealed steels.

Steel designation	Carbon content, (weight %)	Interlamellar spacing of pearlite (λ), (μm) (mean ± standard deviation)
AISI 1005	0.05	0.346 ± 0.049
AISI 1020	0.192	0.263 ± 0.034
AISI 1035	0.35	0.230 ± 0.031
AISI 1050	0.48	0.214 ± 0.035
AISI 1080	0.79	0.204 ± 0.028

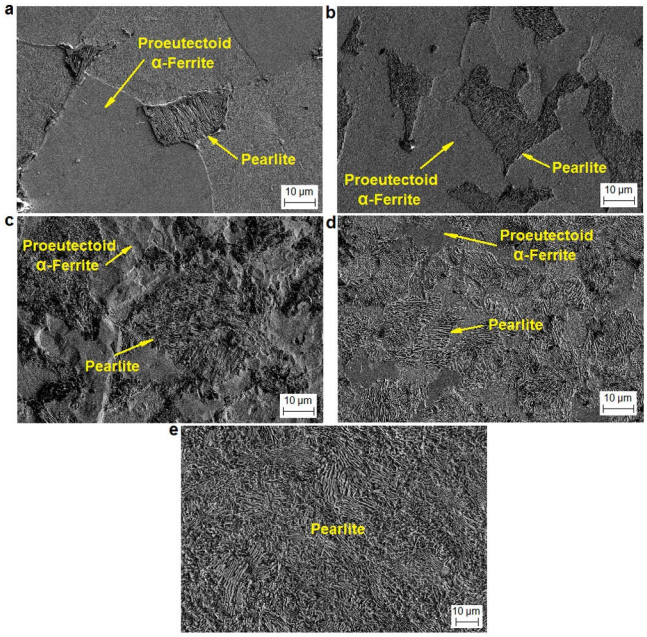

FIGURE 5 Field emission scanning electron micrographs representing overall microstructure of annealed steels containing (a) 0.05 wt.% C, (b) 0.192 wt.% C, (c) 0.35 wt.% C, (d) 0.48 wt.% C, and (e) 0.79 wt.% C.

the time-temperature-transformation diagram of plain carbon steel shifts to right with increasing carbon content up to eutectoid composition [20]. Accordingly, for almost similar pathway of cooling curves pertaining to annealing, the proeutectoid α-ferrite-start temperature (T_{Fs}), proeutectoid α-ferrite-finish temperature (T_{Ff}) and mean temperature for proeutectoid α-ferrite evolution (T_{Fm}) are decreased on shift of time-temperature-transformation diagram to the right, Figure 8. This eventually brings about more degree of undercooling ($\Delta T_{Fm} = A_3 - T_{Fm}$) for proeutectoid α-ferrite evolution, thereby primarily leading to the evolution of finer proeutectoid α-ferrite grains. Furthermore, reduction in annealing temperature (T_A) for same isothermal holding time (1 h) with steels of higher carbon content accounting for relatively finer prior austenite grain may also have secondary effect on the evolution of fine proeutectoid α-ferrite grains. Again, shift of time-temperature-transformation diagram towards right with increase in carbon content up to eutectoid composition results in a reduction in the pearlite-start temperature (T_{Ps}), pearlite-finish temperature (T_{Pf}) and mean temperature for pearlite evolution (T_{Pm}), thereby leading to more degree of undercooling ($\Delta T_{Pm} = A_1 - T_{Pm}$) for pearlite evolution. Accordingly, finer pearlite with reduced interlamellar spacing evolves with increasing carbon content of steel. It is also important to note that the decrease in prior austenite grain size (due to lowering of austenitization temperature (T_A) for a fixed holding time of 1 h) would tend to shift time-temperature-transformation diagram to the left causing a counteracting effect of structural coarsening [20]. However, it appears that in a relatively smaller temperature range of T_A (148 °C, i.e., between 769 °C to 917 °C), the prior austenite grain size reduction effect on the shift of time-temperature-transformation diagram to the left, in turn, 'structural coarsening' effect is relatively small and dominated by the 'structural refining' effect due to shift of time-temperature-transformation diagram to the right owing to higher carbon content.

3.2 | Hardness of different microconstituents

The trend in hardness variation of individual microconstituents as ascertained by microhardness test at low load (25 gf) indicates toward an enhanced hardness of proeutectoid α-ferrite (H_{PF}) and pearlite (H_P) with increasing carbon content of annealed steel, Table 6, Figure 9. This is essentially attributed to the reduction in grain size (D) of proeutectoid α-ferrite and the reduction in interlamellar spacing (λ) of pearlite with increasing carbon content of annealed steel.

The structure-property correlation in steel is usually expressed in terms of Hall-Petch type relationship [22, 23, 29].

$$H_{PF} = H^{\circ}_{PF} + K_{PF} D^{-0.5} \quad (3)$$

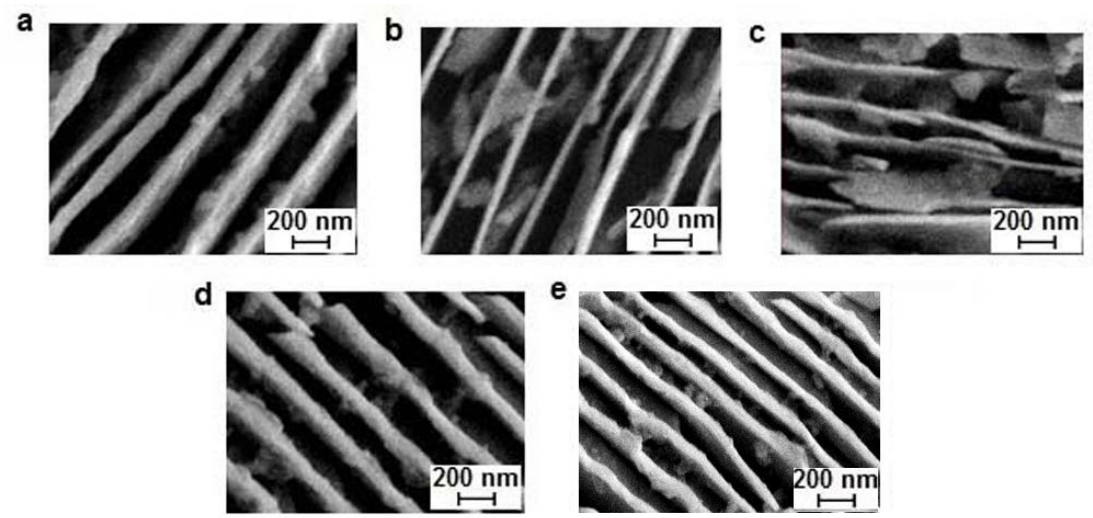

FIGURE 6 Field emission scanning electron micrographs depicting pearlite region at high magnification in annealed steels containing (a) 0.05 wt.% C, (b) 0.192 wt.% C, (c) 0.35 wt.% C, (d) 0.48 wt.% C, and (e) 0.79 wt.% C.

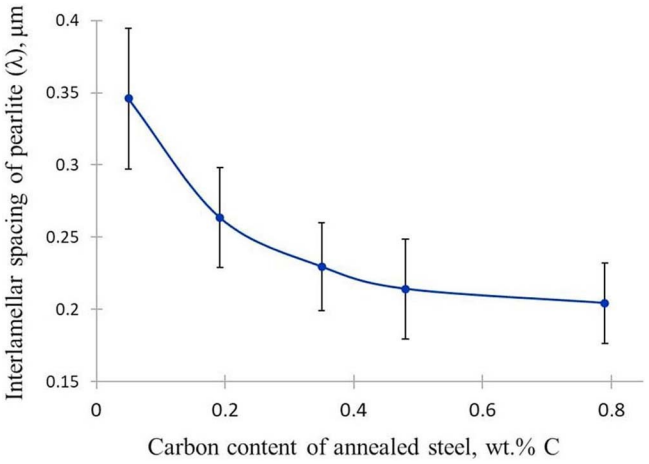

FIGURE 7 Variation of interlamellar spacing of pearlite with carbon content of annealed steel.

$$H_P = H^\circ_P + K_P \lambda^{-0.5} \quad (4)$$

Where, H°_{PF}, K_{PF}, H°_P and K_P are constants specific to the system considered. In order to find out these system specific constants so as to obtain complete empirical relationships, H_{PF} versus $D^{-0.5}$ and H_P versus $\lambda^{-0.5}$ plots are generated and fitted to straight line with reasonable accuracy (coefficient of determination, $R^2 > 0.9$) using Microsoft Excel Software, Figures 10, 11. The resultant final empirical relationships are enumerated below.

$$H_{PF} = 87.067 + 237.6D^{-0.5} \quad (5)$$

$$H_P = 40.323 + 100.18\lambda^{-0.5} \quad (6)$$

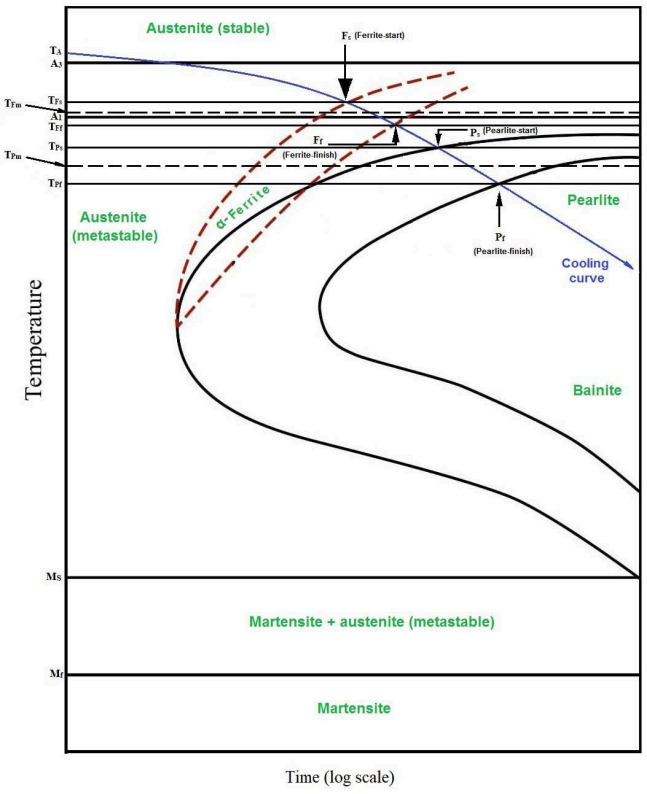

FIGURE 8 A scheme of cooling curve superimposed on the time-temperature-transformation (TTT) diagram of hypoeutectoid steel.

Where, D and λ are in μm; while H_{PF} and H_P are the Vickers hardness values (in kg mm^{-2}).

Furthermore, it is important to note that a gradual hardness variation for both proeutectoid α-ferrite and pearlite is observed in view of fundamental structure-property correlation resulting in an impact on overall

TABLE 6 Microhardness test results enumerating hardness of different microconstituents.

Steel designation	Carbon content, (weight %)	Microhardness test results	
		Hardness of proeutectoid α-ferrite region (H_{PF}), HV 0.025 (mean ± standard deviation)	Hardness of pearlite region (H_P), HV 0.025 (mean ± standard deviation)
AISI 1005	0.05	115 ± 2	210 ± 5
AISI 1020	0.192	124 ± 2	237 ± 3
AISI 1035	0.35	132 ± 1	248 ± 2
AISI 1050	0.48	137 ± 2	255 ± 2
AISI 1080	0.79	Not applicable	264 ± 3

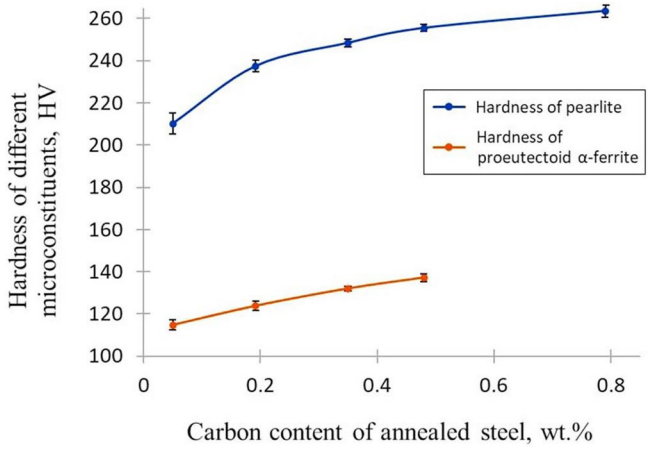

FIGURE 9 Variation of the hardness of individual microconstituents with carbon content of annealed steels.

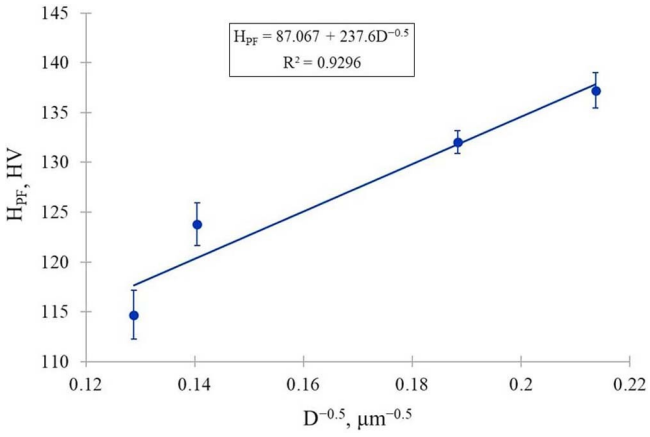

FIGURE 10 Variation of H_{PF} with $D^{-0.5}$.

hardness of annealed plain carbon steel as a function of carbon content.

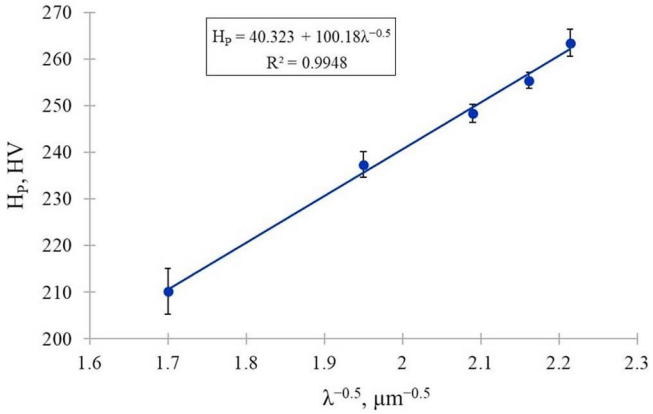

FIGURE 11 Variation of H_P with $\lambda^{-0.5}$.

3.3 | Overall hardness

The cumulative effect of hardness values of the individual microconstituents on overall hardness (H) of annealed steel may be conceived in terms of rule of mixture as given below [30].

$$H = f_{PF}H_{PF} + f_PH_P \tag{7}$$

Combining equation (1), (2), (5) and (6) we get:

$$H = \left(\frac{0.8 - X}{0.8 - 0.025}\right) \times (87.067 + 237.6D^{-0.5}) + \left(\frac{X - 0.025}{0.8 - 0.025}\right) \times (40.323 + 100.18\lambda^{-0.5}) \tag{8}$$

Accordingly,

$$H = (245.26 - 306.58X)\ D^{-0.5} + (-3.16 + 129.26X)\ \lambda^{-0.5} - 60.31X + 88.57 \tag{9}$$

TABLE 7 Experimentally measured overall hardness values of annealed steels in comparison with those obtained through the developed empirical relationship.

Steel designation	Carbon content, (wt.%)	Experimentally measured overall hardness (H_{ex}), HV 2 (mean ± standard deviation)	Overall hardness as obtained from developed empirical relationship (H) as per Eq (9), HV	% deviation with respect to experimentally measured overall hardness $\left(\left\|\frac{H_{ex}-H}{H_{ex}}\right\| \times 100\right)$
AISI 1005	0.05	116 ± 1	121	4.3
AISI 1020	0.192	147 ± 2	145	1.4
AISI 1035	0.35	180 ± 1	181	0.6
AISI 1050	0.48	203 ± 2	208	2.5
AISI 1080	0.79	260 ± 2	260	Negligible

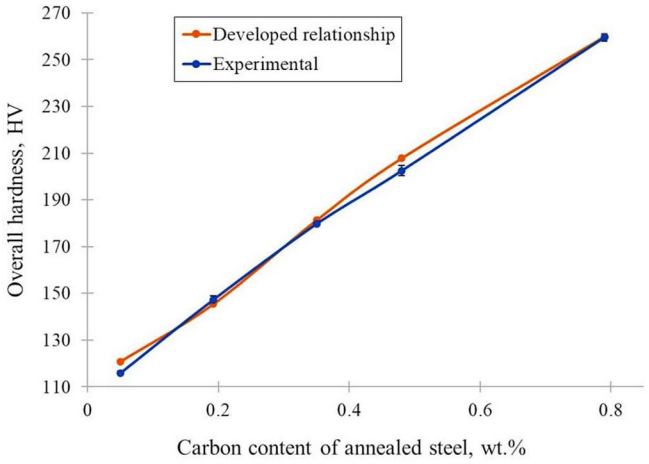

FIGURE 12 Overall hardness values of annealed steels with respect to carbon content as measured experimentally and as obtained through the developed empirical relationship.

Equation 9 is the final empirical relationship developed for the overall Vickers hardness (H) of annealed plain carbon steel in correlation to chemistry (X, the weight% carbon present in steel) and microstructure (D, the average grain diameter of proeutectoid α-ferrite phase in μm; and λ, the interlamellar spacing of pearlite in μm). In order to justify this relationship, the overall hardness values of all steel specimens have been measured in the same hardness testing machine at the highest load available (2 kgf) in comparison with the hardness values calculated by the developed relationship, Equation 9, Table 7, Figure 12. Overall hardness increases with increase in carbon content of annealed plain carbon steel due to associated structural refinement (reduction in D and λ). Moreover, the hardness values obtained from the developed relationship, Equation 9, closely follows the experimentally obtained overall hardness values with very small deviation (% deviation $\ll 10$). This justifies the significance of the developed relationship, Equation 9, which is formulated for the first time in this study, judiciously correlating overall hardness, weight% carbon, grain size of proeutectoid α-ferrite and interlamellar spacing of pearlite.

The developed empirical relationship that theoretically correlates overall hardness with microstructural parameters (grain size and interlamellar spacing) has its own fundamental origin. This origin stems from at first using the Hall-Petch relationship, a well-known fundamental equation to correlate hardness values of individual microstructural features with grain size or interlamellar spacing. The hardness values of the individual microstructural features are obviously experimentally obtained in terms of microhardness measurement at low load so as to find out the unknown Hall-Petch constant parameters through curve fitting for this particular system. Thereafter, the overall hardness is theoretically predicted using 'Rule of mixture' along with the representation of volume fraction of different microconstituents with regard to alloy chemistry (carbon content) by invoking 'Lever rule' (another fundamental relationship). Finally this theoretically predicted overall hardness is correlated with the experimentally measured overall hardness to substantiate the validity of developed relationship. Using this unique relationship one can straightway obtain the overall hardness of steel (an important material property) from the known chemistry and microstructural parameters. Further analytical model may be developed to justify the values of Hall-Petch parameters as a futuristic work.

4 | CONCLUSION

1. Even in similar condition of cooling (furnace cooling) pertaining to the full annealing treatment, microstructural modifications of individual microconstituents are feasible with varying chemistry (carbon content) of plain carbon steel.

2. Structural refinement of both the prime microconstituents (proeutectoid α-ferrite and pearlite) is found to be aggravated with increasing carbon content of annealed steels till eutectoid composition.
3. Hall-Petch type relationship is abided by the relationship between hardness and microconstituent-size, both in terms of the grain size of proeutectoid α-ferrite and the interlamellar spacing of pearlite.
4. In accordance, following the rule of mixture, an empirical relationship is developed for the first time to connect overall hardness, carbon content, grain size of proeutectoid α-ferrite and interlamellar spacing of pearlite in view of ascertaining chemistry-structure-property correlation in annealed plain carbon steel.
5. The developed relationship is found to closely follow the experimental results, thereby envisaging its utility for application in the future.

ORCID

J. Maity http://orcid.org/0000-0002-3798-4205

REFERENCES

1. A. G. Guy, *Metall. Trans.* **1972**, *3*, 2535.
2. H. K. D. H. Bhadeshia, L. E. Svensson, Mathematical Modelling of Weld Phenomena, (Ed.) H. Cerjak, K. E. Esterling, Institute of Materials, 109–182, London, **1993**.
3. F. C. Hull, R. F. Mehl, *Trans. ASM.* **1942**, *30*, 381.
4. R. F. Mehl, *Metallogr. Microstruct.Anal.* **2015**, *4*, 423.
5. D. Phelan, R. Dippenaar, *Metall. Trans. A* **2004**, *35A*, 3701.
6. Z. Nishiyama, Martensitic Transformation, (1st Ed.), Academic Press, New York, **1978**.
7. H. K. D. H. Bhadeshia, D. V. Edmonds, *Acta Metall. Mater.* **1980**, *24*, 1265.
8. A. Saha, D. K. Mondal, J. Maity, *J. Mater. Eng. Perform.* **2011**, *20*, 114.
9. A. Saha, D. K. Mondal, J. Maity, *Mater.Sci. and Eng.A* **2010**, *527*, 4001.
10. A. Saha, D. K. Mondal, K. Biswas, J. Maity, *Mater. Sci. and Eng.A* **2012**, *534*, 465.
11. A. Saha, D. K. Mondal, K. Biswas, J. Maity, *Mater. Sci. and Eng.A* **2012**, *541*, 204.
12. J. Maity, A. Saha, D. K. Mondal, K. Biswas, *Philos. Mag. Lett.* **2013**, *93*, 231.
13. S. Maji, A. R. Subhani, B. K. Show, J. Maity, *J. Mater. Eng. Perform.* **2017**, *26*, 3058.
14. A. R. Subhani, D. K. Mondal, C. Mondal, J. Maity, *Philos. Mag. Lett.* **2018**, *98*, 240.
15. A. R. Subhani, D. K. Mondal, C. Mondal, H. Roy, J. Maity, *J. Mater. Eng. Perform.* **2019**, *28*, 2192.
16. P. Biswas, J. Maity, *Arch. Metall. Mater.* **2020**, *65*, 1171.
17. M. Mallick, S. K. Mitra, D. Basak, N. K. Roy, J. Maity, *Philos. Mag.* **2021**, *101*, 555.
18. M. Mallick, S. K. Mitra, D. Basak, N. K. Roy, J. Maity, *Steel Res. Int.* **2021**, *92*, 1.
19. M. Mallick, B. Hazra, S. K. Mitra, D. Basak, B. K. Show, J. Maity, *J. Mater. Eng. Perform.* **2022**, *31*, 3661.
20. C. R. Brooks, *Principle of the Heat Treatment of Plain Carbon and Low Alloy Steels* ASM International, Ohio, **1996**.
21. H. K. D. H. Bhadeshia, R. Honeycombe, Steels: Microstructure and Properties, (3rd Ed.), Butterworth-Heinemann, Boston, **2006**.
22. E. O. Hall, *Proc. Phys. Soc. London B.* **1951**, *64*, 747.
23. N. J. Petch, *J. Iron Steel Inst.* **1953**, *174*, 25.
24. N. Hansen, *Scripta. Mater.* **2004**, *51*, 801.
25. K. W. Andrews, *J. Iron Steel Inst. Jpn.* **1965**, *203*, 721.
26. X. Xie, *Steel Heat Treatment Hand Book*, in: G. E.Totten, M. A. H. Howes (Eds.), Marcel Dekker, 990–995, New York, **1997**.
27. A. Ghosh, S. Das, S. Chatterjee, P. R. Rao, *Mater. Charact.* **2006**, *56*, 59.
28. M. Ali, D. Porter, J. Ko, M. Eissa, H. E. Faramawy, T. Mattar, *J. Iron Steel Res. Int.* **2019**, *26*, 1350.
29. S. Sadeghpour, *International Journal of Iron and Steel Society of Iran* **2011**, *8*, 1.
30. M. Alibeyki, H. Mirzadeh, M. Najafi, A. Kalhor, *J. Mater. Eng. Perform.* **2017**, *26*, 2683.

How to cite this article: J. Maity, S. A. Rahman, S. Alam, K. K. Singh, P. Kumar, S. Hembram, *Materialwiss. Werkstofftech.* **2023**, *54*, e202200184. https://doi.org/10.1002/mawe.202200184